Superconductivity 9 (2024) 100085

Contents lists available at ScienceDirect

Superconductivity

journal homepage: www.elsevier.com/locate/supcon

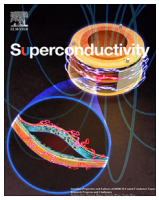

Full Length Article

Short circuit analysis of a fault-tolerant current-limiting high temperature superconducting transformer in a power system in presence of distributed generations

Alireza Sadeghi, Shahin Alipour Bonab, Wenjuan Song, Mohammad Yazdani-Asrami *

Propulsion, Electrification & Superconductivity Group, Autonomous Systems & Connectivity Division, James Watt School of Engineering, University of Glasgow, Glasgow G12 8QQ, United Kingdom

ARTICLE INFO

Keywords:
Fault Energy
Heat dissipation
Heat transfer
Insulation
Recovery Time
Temperature rise

ABSTRACT

Power transformers are key elements for the safe and reliable delivery of electrical energy generated by renewable energy resources to consumers via transmission lines. Fault-tolerant current-limiting High Temperature Superconducting (FTCL HTS) transformers are type of superconducting transformers that tolerate fault for seconds and limit the fault current without the threat of burnout or delamination of tapes and deformation of windings. In this paper, the fault performance of a FTCL HTS transformer in a standard IEEE power system is investigated. The studied transformer is a 50 MVA 132 kV/13.8 kV transformer where both windings are made up of HTS tapes. The understudied power system consists of two microgrids with distributed generators. Part of the power in microgrids is supplied by the upstream grid which is connected to the microgrids through the HTS transformers. Two fault scenarios have been considered in this power system, in each one of these scenarios, a fault happens in one of the microgrids. Two considered fault scenarios have an approximate fault current of 18x to 23x of the rated current in the secondary windings. Results showed that insulated windings in FTCL HTS transformers could substantially reduce the peak temperature of the HTS windings, compared to bare windings. Afterwards, post-fault loading is imposed on the HTS windings, to observe their performance against the current increase after fault clearance. In this case, for the first scenario of the faults, the FTCL HTS transformer could tolerate 192% of post-fault overloading, while this number for the second fault scenario is 170%. Finally, the impact of post-fault loading on the full recovery time was discussed.

1. Introduction

During the last few years, the amount of greenhouse gas emissions has increased, that resulted in increase of Earth's bulk temperature. To avoid this, “Net Zero” concept has been proposed, which focuses on greenhouse gas emission neutrality until 2050 [1]. The thermal power plants and the transportation sectors are among the sources of greenhouse gas emissions [2,3]. In power systems, the integration of renewable energy resources, such as offshore wind farms or solar farms, is proposed as a solution. For instance, the capacity of wind farms in the UK was only 2.5 GW before 2012, and now it is approximately 11 GW [4]. Typically, offshore wind farms harvest 8 MW to 13 MW of electrical power per turbine.

Transformers play crucial role in uninterruptable delivery of harvested energy to the loads. To do this, large conventional copper-based transformers exhibit a high amount of loss, heavy weight, large footprint, vulnerability against transients and harmonics, and high cost [5–7]. To tackle these issues, High Temperature Superconducting (HTS) transformers were proposed which offer lower loss, lighter weight, and lower total ownership cost [8–11]. Important challenges of HTS transformer implementation in power networks are AC loss and fault performance. AC loss-related analysis has been discussed in the literature [12–28]. The importance of fault performance of HTS transformers is that superconducting coated conductors are fragile against faults. Thus, by high amplitude short circuit currents, the heat generated in tapes abruptly increases, and consequently, the winding temperatures might burn out [29,30]. This makes the fault performance analysis of HTS transformers as an important step towards their full commercialization [31].

In this regard, reference [32], the fault current limitation capability of a 64 MVA HTS transformer was discussed to show how HTS transformers could be used to limit the fault current imposed on the power

* Corresponding author.
E-mail address: mohammad.yazdani-asrami@glasgow.ac.uk (M. Yazdani-Asrami).

https://doi.org/10.1016/j.supcon.2024.100085
Received 15 December 2023; Revised 29 January 2024; Accepted 30 January 2024
Available online 3 February 2024

system. In this reference [32], the impedance of the HTS transformer during fault is compared with the impedance of a copper-based transformer with the same ratings. Results showed that in the presence of the HTS transformer, 89% of the fault current is limited. However, a discussion on the thermal characteristics of the HTS transformer is missing. The fault performance of a 1 MVA HTS transformer was studied in [33] concerning the thermal characteristics of an HTS transformer. This study aimed to show how changes in the thermal mass of different layers in the HTS coated conductor would impact the fault performance of the HTS transformer. The results showed that the temperature of windings could reach to maximum of 600 K which results in their burnout, however; no solution was proposed for that. An Equivalent Circuit Model (ECM) is used in [34] which characterizes the fault performance of a 10 kVA, 230 V/115 V HTS transformer under a three-phase short circuit fault. The presented results showed that the ECM model has an excellent agreement with the numerical model. Also, it is shown that under the applied fault, the windings of the HTS transformer could burn out, especially low voltage windings. The impact of inrush currents was discussed in [35]. The properties of superconducting tapes such as the thickness of stabilizers and the substrates could have a direct impact on the fault performance of HTS tapes, which is analysed and discussed in [36,37]. The impact of changing the structure of the HTS tapes and their effect on the Fault Current Limiting (FCL) capability of HTS transformers is discussed in [38–42]. For this purpose, the thermal mass and electric conductivity of substrate and stabilizer layers have been changed by increasing the thickness of these sublayers and changing their materials. The results have shown that FCL HTS transformers could suppress the fault current, however, their main problem is still the rapid temperature rise. To address the issue of temperature, increase in FCL HTS transformers, another type of HTS transformers has been proposed, known as Fault Tolerant Current Limiting (FTCL) HTS transformers in [43]. These transformers not only limit the fault current, but the temperature increase rate would be limited to avoid thermal runaway or burnouts by increasing the heat transfer from the tape surface to the coolant [44]. Usually, in this type, the heat transfer ratio is increased by using different types of dielectrics to cover the HTS tapes, also lowering the operating temperature of the coolant, and structural changes of the HTS tapes have a direct impact on the peak temperature of HTS transformers. Experimental tests have shown that FTCL HTS transformers could endure a massive fault current for 2 seconds without the possibility of burnout [43]. Experimentally validated models have shown that such HTS transformers could be recovered even when 225% of loading is applied to the HTS transformer after fault clearance [45]. The characterization of FTCL HTS transformers has been discussed in the literature, however, their system-level study is still missing. The system-level study allows a comprehensive understanding of the HTS transformer's behaviour when interacting with different components of the power system. It also shows the interdependencies in different components of power systems where these interdependencies could predict that how changes in the power system, could impact the characteristics of FTCL HTS transformer.

In this paper, a 50 MVA 3-phase FTCL HTS transformer was considered for the system-level study of HTS transformers in a benchmark power system of the IEEE Standard 399–1997, presented in [46,47]. This study aims to show how FTCL HTS transformers would behave under real fault scenarios. Three types of winding for FTCL HTS transformers were discussed in this paper, namely, HTS transformers with bare tapes, Kapton insulated tapes, and solid insulated tapes. The results have shown that by using insulations, the peak temperature of HTS windings is 34% to 72% reduced, compared to bare HTS windings. Also, an HTS transformer with solid insulated windings could tolerate 170% to 192% of overloading after fault clearance. This means that overloading could be tolerated by the HTS transformer, even when the temperature is higher than the operational temperature. As a result of this, exactly after fault clearance, the HTS transformer could deliver the power to the grid.

2. Modelling methodology

In this paper, studied HTS transformer is characterized through an ECM, where electrical components are used to determine the thermal, magnetic, and electric characteristics of HTS tapes, as well as the windings behaviour. The ECM of a 3-phase HTS transformer is illustrated in Fig. 1, where Fig. 1(a) shows the ECM of HTS tapes used in windings of the HTS transformer while Fig. 1(b) shows the ECM of the whole HTS transformer including the iron core. To develop such a model, one must first conceive the characterization performance of an HTS transformer, and then, translate the characteristic into the circuit-based components such as resistors, inductances, and capacitances. The procedure of characterization and modelling by ECM is shown in Fig. 2.

It should be noted that electrically, any HTS transformer could operate in three operational states, which are steady-state, transient-state, and recovery-state. The flowchart shown in Fig. 3 shows the modelling procedure of the HTS transformer. The first step is getting the design and operational properties of the HTS transformer, as well as the features of superconducting tape sub-layers. Then, the current at each time step is measured, if the current is higher than the critical current of the HTS winding, the HTS transformer is operating in a transient state without any need for measuring the temperature. However, if the current is lower than the critical current, it does not mean that the transformer is operating in a steady state. This is because the temperature could be higher than the critical temperature of HTS tapes which means the recovery state is going on. Finally, if both current and temperature are lower than their critical values, the HTS transformer is working in a steady-state.

Equation (1) calculates the equivalent resistance of the HTS tapes and equation (2) calculates the temperature and current dependent characteristic of the superconducting sublayer in HTS tape [48].

$$\rho_{tape} = \left(\frac{1}{\rho_{sc}} + \frac{1}{\rho_{stab}} + \frac{1}{\rho_{sub}} + \frac{1}{\rho_{ag}}\right)^{-1} \tag{1}$$

$$\rho_{sc}(J,T) = \begin{cases} \rho_0 & J < J_c(T) \\ \rho_0 + \left(\frac{E_0}{J}\right)\left(\frac{J}{J_c(T)} - 1\right)^n & J < J_c(T) < 3J_c(T) \\ \dfrac{(\rho_{sat})\left(\left(\frac{E_0}{J}\right)\left(\frac{J}{J_c(T)}-1\right)^n\right)}{(\rho_{sat}) + \left(\rho_0 + \left(\frac{E_0}{J}\right)\left(\frac{J}{J_c(T)}-1\right)^n\right)} & J > 3J_c(T) \end{cases} \tag{2}$$

where, ρ_{sc} is the resistivity of the superconducting sublayer, ρ_{stab} is the resistivity of stabilizer, ρ_{sub} is the resistivity of substrate, ρ_{ag} is the resistivity of the silver layer in HTS tape, ρ_0 is the resistivity of Yttrium Barium Copper Oxide (YBCO) tapes in steady-state, E_0 is the electric field, J is the current density, $J_c(T)$ is the critical current density, n is the index value, and ρ_{sat} is the saturation resistance [49].

Self and mutual inductances of HTS windings are calculated by using equations (3) and (4) [50,51,21]:

$$L_i = \frac{N_i^2 \mu_0 \mu_r A_F}{\ell} \tag{3}$$

$$M_{ij} = \frac{N_i N_j \lambda_i}{I_j} \tag{4}$$

where, N_i is the turn number, μ_0 is the permeability of free space equal to $4\pi \times 10^{-7}$H/m, μ_r is relative permeability of the core material, A_F is the cross-section area of the flux path, ℓ is the height of the windings, λ_i is the flux linkage of layer i, and I_j is the excitation current of winding j.

For determination of magnetic field in different locations of HTS windings the equations (5) and (6) could be used [52,22]:

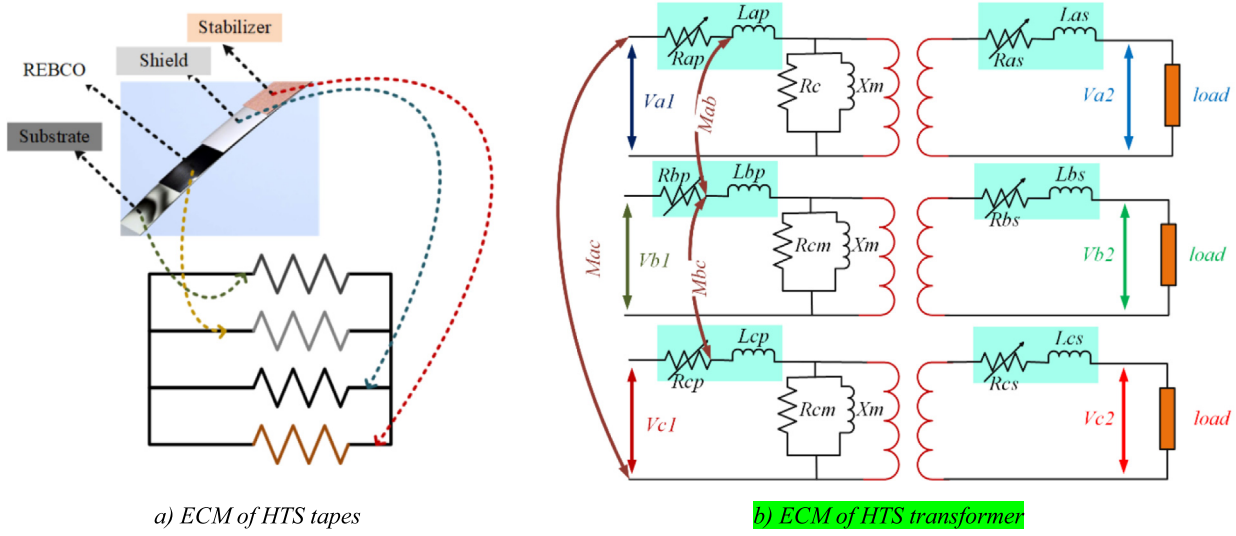

Fig. 1. The equivalent circuit model used for characterising the HTS transformer, referenced from the Primary Side.

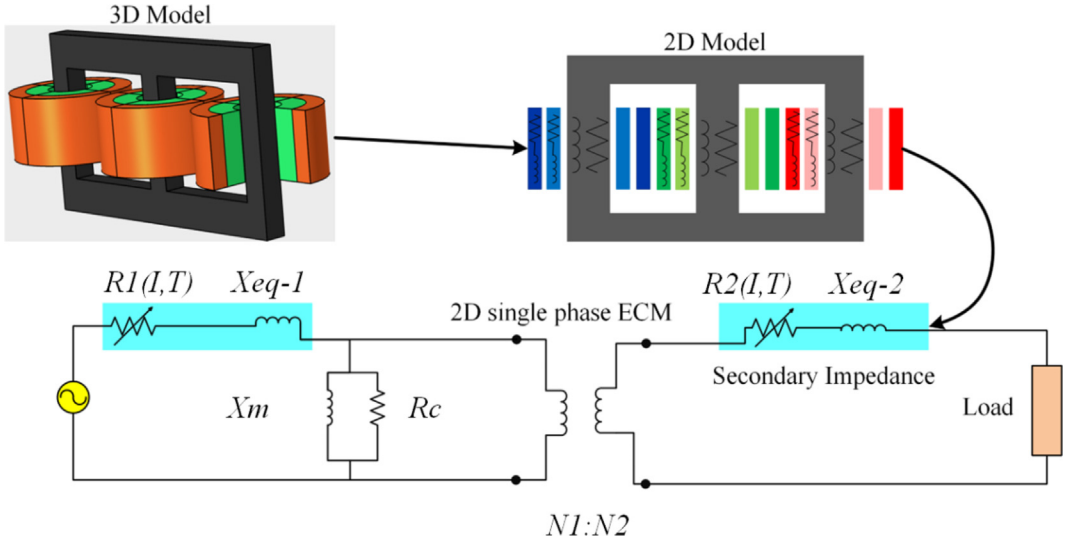

Fig. 2. Modelling procedure of HTS transformer using ECM.

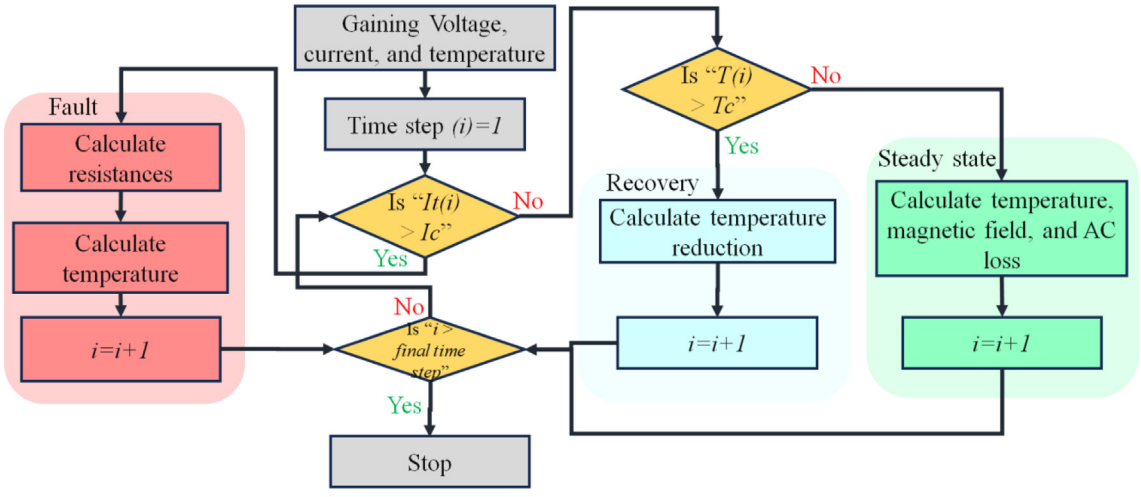

Fig. 3. Flowchart of Modelling procedure by ECM in HTS transformer.

$$B_{ax} = \frac{1}{\sqrt{2}\pi}\frac{\mu_0 I(t) N}{\ell}\left|tan^{-1}\frac{z_j+\frac{\ell}{2}}{r_i} - tan^{-1}\frac{z_j-\frac{\ell}{2}}{r_i}\right| \quad (5)$$

$$B_r = \frac{1}{2\sqrt{2}\pi}\left[ln\left(\left(\frac{2r_i}{\ell}\right)^2 + \left(\frac{2z_j}{\ell}-1\right)^2\right) - ln\left(\left(\frac{2r_i}{\ell}\right)^2 + \left(\frac{2z_j}{\ell}+1\right)^2\right)\right] \quad (6)$$

where, $I(t)$ is the RMS current passing through the HTS windings and ℓ is the coil height.

The calculation method for perpendicular and parallel magnetic field in HTS transformer based on the axial magnetic and radial fields are shown in equations (7) and (8) which are based on the winding angle Θ [52]:

$$B_{\parallel} = B_{ax}\cos\Theta + B_r \sin\Theta \quad (7)$$

$$B_{\perp} = B_{ax}\sin\Theta + B_r \cos\Theta \quad (8)$$

The losses in HTS transformers must be calculated for the sake of heat load determination and gaining the value of temperature change. For this purpose, equations (9) to (15) are used which show the losses resulted by self-magnetic field, parallel magnetic field, perpendicular magnetic field, current lead, cryostat, and the iron core, respectively [53].

$$Q_{sf} = \frac{fI_c}{\pi}\mu_0\left(lnF_i - F_i lnF_i + F_i - \frac{1}{2}F_i^2\right) \quad (9)$$

$$F_i = \frac{I_{op}}{I_c} \quad (10)$$

$$Q_{\parallel} = \begin{cases} \frac{fCA_c}{\mu_0}\frac{2B_{\parallel}^3}{3B_P} & B_{\parallel} < B_P \\ \frac{fCA_c}{\mu_0}\left(2B_P B_{\parallel} - \frac{4}{3}B_P^2\right) & B_{\parallel} > B_P \end{cases} \quad (11)$$

$$Q_{\perp} = Kf\omega^2\frac{\pi}{\mu_0}B_C B_{\perp}\left[ln\left(cosh\frac{B_{\perp}}{B_C}\right)^{\frac{2B_C}{B_{\perp}}} - tanh\frac{B_{\perp}}{B_C}\right] \quad (12)$$

$$Q_{CL} = 6q_{CL}(I_{LV} + I_{HV}) \quad (13)$$

$$Q_{cryo} = \frac{A_{cryo}\Delta T}{\delta_{ins}}\lambda_{ins} \quad (14)$$

$$Q_{core} = 1.2\mathbb{C}_P G_{core} \quad (15)$$

where, f is frequency, I_c is critical current, C is the ratio between the superconductor cross section and the total tape cross section, B_P is the full penetration flux density, A_c is the total tape cross section, B_c is the critical field, K is a geometrical parameter, w is the tape width, q_{cl} is the specific thermal income per unit current [15], I_{LV} is current at low voltage side, I_{HV} is the current at high voltage side (in kA), λ_{ins} is thermal conductivity of cryostat, δ_{ins} is the thermal insulation thickness, A_{cryo} is the cryostat surface, G_{core} is the weight of the core, and $\mathbb{C}_P$ is the loss per unit weight of ferromagnetic material [53].

By having the values of total heat load in each time step, the thermal characteristic of the HTS transformer could be determined based on equation (16) [54]:

$$D(T)C_p(T)\frac{\partial T}{\partial t} = k(T)\frac{\partial^2 T}{\partial x^2} + Q - \nabla q \quad (16)$$

where, $D(T)$ is the density of the material in (kg/m^3), $C_p(T)$ is the specific heat capacity in J/kg.K, $k(T)$ is the thermal conductivity in W/m.K, Q is the total generated heat in windings of HTS transformer, and ∇q is the heat flux in bath cooling which could be translated as the amount of heat transferred from the surface of the superconductor to the coolant fluid, under pool boiling conditions. During steady state, Q is equal to the losses calculated in equations (9) to (15) while under transient states, Q equals to the amount of Joule loss generated in stabilizers of HTS tapes in transformer winding. For the determination of the heat flux, more equations and details have been discussed in [45].

3. Results and discussions

In this section, the configuration of the power system is introduced where the HTS transformer is implemented in. The characteristic of the HTS transformer, during normal conditions in this power system is analysed. The fault performance of the HTS transformer covered with different insulation materials as well as bare tapes is analysed. The best fault tolerability performance of an HTS transformer with insulated windings is discussed more in terms of recovery under load.

3.1. Power grid configuration, specifications, and fault scenarios

In this paper, a standard power system, i.e., IEEE Standard 399-1997 is considered to analyse the fault performance of the HTS transformer under power system conditions in the presence of the Distributed Generators (DGs). Here DGs are synchronous generators that supply part of power for the related loads in the microgrids (MG). This means that DG1 supplies part of the electric power required by Load 1 and Load 2 while DG2 is responsible for supplying Load 3 and Load 4, as shown in Fig. 4. The power system consists of three main parts, as shown in Fig. 4, the upper part which has two Points of Common Coupling (PCC), a capacitor bank, a load, and an HTS transformer. Other parts of the grid are two Microgrids, i.e., MG1, and MG2, each of which has two loads and a DG. The voltage of the HTS transformer is 132 kV/13.8 kV which makes the reference voltage of the understudied grid to be 13.8 kV. The MGs are connected to the main grid through a PCC which is a Circuit Breaker (CB), when MGs need to inject into/receive power from upper hand grid, the CB is closed. In the case of islanding opertional mode, CB would be open. In this concept, islanding refers to the operation condition of MGs where their generated power is equal to consumed power, thus, they do not need to inject/receive the power to/from the upper hand power system [55]. The details of the power system are tabulated in Table 1 and more information is discussed in [46,47]. The aim of considering these two load scenarios is to investigate whether a fault occurring in one of the MGs would still allow the HTS transformer to provide the required power for another MG that experiences no faults. As seen in Fig. 4, when F1 happens, MG1 is still operating and power should be supplied, this is also the case with F2 fault and MG2.

The HTS transformer is a 50 MVA transformer with an X/R ratio approximately equal to 22, where YBCO-based coated conductors are used in its windings. This HTS transformer operates at 65 K base temperature which is cooled down by sub-cooled liquid nitrogen. The electrical properties of this HTS transformer are tabulated in Table 2, the design of transformer is shown in Table 3, and the properties of HTS tapes are listed in Table 4.

Fig. 5 shows the DG's start-up current and the steady-state operation of the grid, after the transients are damped, the shown current is measured on the secondary side of the HTS transformer. As seen in this figure, when the DGs start to work, a current, higher than the rated current, is injected into the power system as well as the HTS transformer, after 2 seconds the transient current is damped and the current finally enters its steady state. The HTS transformer is designed so that the starting current does not cause the thermal deterioration of the YBCO tapes. As shown in Fig. 6, the maximum temperature of phases A, B, and C regarding the starting current is about 65.8 K which is just about 1% higher than the maximum temperature of these phases at steady state.

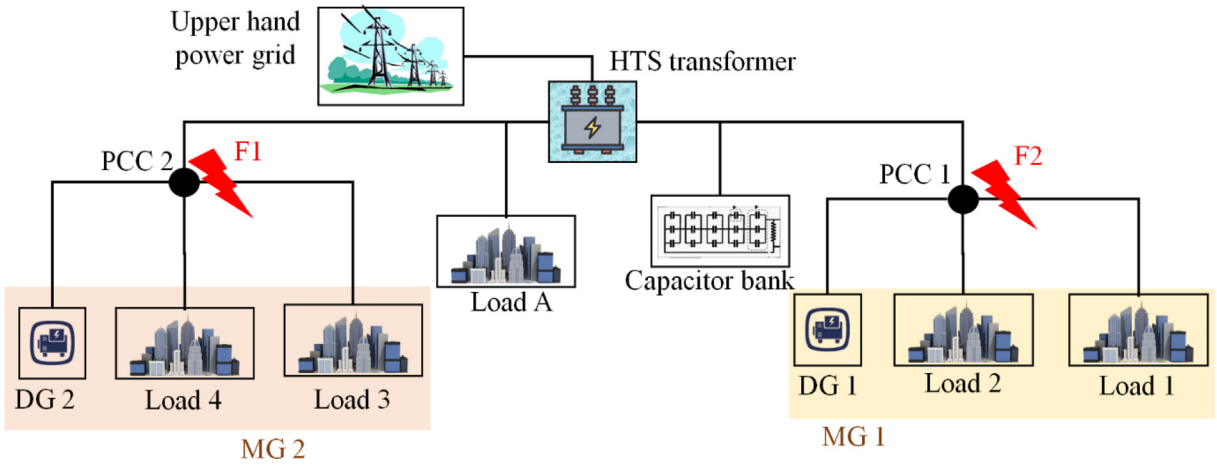

Fig. 4. A schematic of a power system where two Micro Grids (MGs) have been considered and the power is delivered to the system through an HTS transformer.

Table 1
The specifications of the power system consisting of an HTS transformer.

Parameter	Value	Unit
Voltage of DG2	13.8	kV
Generated power by DG2	2.5	MVA
Active power of load 4	0.9	MW
Active power of load 3	0.9	MW
Reactive power of load 3	0.6	MVAr
Active power of load A	3.2	MW
Reactive power of load A	1.9	MVAr
Reactive power of capacitor bank	1.5	MVAr
Voltage of DG1	13.8	kV
Generated power by DG1	5	MVA
Active power of load 2	1.5	MW
Reactive power of load 2	1.0	MVAr
Active power of load 1	0.8	MW
Reactive power of load 1	0.47	MVAr
Fault timing 1	4 to 4.1	s
Fault timing 2	4.5 to 4.6	s

Table 2
The specifications of the 50 MVA HTS transformer [56].

Parameter	Primary side	Secondary side	unit
Nominal voltage	132	13.8	kV
Number of strands	8	17	-
Nominal current	480	2250	A
Number of turns	860	156	-
Number of layers	10	4	-
Gap between layers	0.05	0.025	mm
Turns per layer	86	39	-
Windings critical current	740	3400	A
Maximum flux density in the core	1.6		T
Loading safety factor of windings	65%		
Total leakage reactance	0.067		p.u.
Magnetisation reactance	105		p.u.

Table 3
Design summary of 50 MVA HTS transformer [56].

Description	Value (mm)
Core radius	300
High voltage winding details	
Radius to midpoint	402.5
Height	516
Radial build	21.5
Low voltage winding detail	
Radius to midpoint of inner winding	364.5
Radius to midpoint of outer winding	440.5
Height	507
Radial build	8.7
Gap between adjacent windings	23
Clearance between windings and Core	
Upper	300
Lower	300
Radial space between inner LV winding and core	60
Radial space between inner LV winding and outside of cryostat	40
Separation between adjacent phase cryostats	30
Gap between coils and core on top	300
Gap between coils and core on bottom	300
Gap between adjacent windings	23

Table 4
The properties of YBCO coated conducted used in winding of HTS transformer [56].

Parameter	Value/type	Unit
Critical current @ 65 K & 0 T	260	A
Index value @ 65 K & 0 T	28	-
Tape width	4.4	mm
Tape thickness	100	μm
Stabiliser thickness	40	μm
Stabiliser material	Copper	-
Shield thickness	3.8	μm
Shield material	Silver	-
Substrate thickness	50	μm
Substrate material	Hastelloy	-
Superconducting thickness	1	μm
Superconducting material	YBCO	-

Fault scenarios are imposed in MGs where the fault resistance is 0.01 Ω, and their impact on the HTS transformer is going to be discussed. As shown in Fig. 7, fault scenario 1, imposes approximately 40 kA fault current to the grid while scenario 2 imposes 50 kA fault current to the grid.

This investigation aims to see how different fault scenarios would increase the windings temperature of the HTS transformer. If the HTS transformer does not face burnouts in two fault scenarios, it can supply the required power of healthy MG when the other one is experiencing a short circuit fault. In this regard, burnout happens when the temperature of superconducting tapes/windings surpasses the 300 K limit [44]. Under such condition, superconducting properties of the tapes/windings are compromised, or they are deformed due to exposure to excessive harsh thermal conditions. In other words, the HTS material essentially loses its ability to superconduct effectively and may even undergo irreversible changes [44].

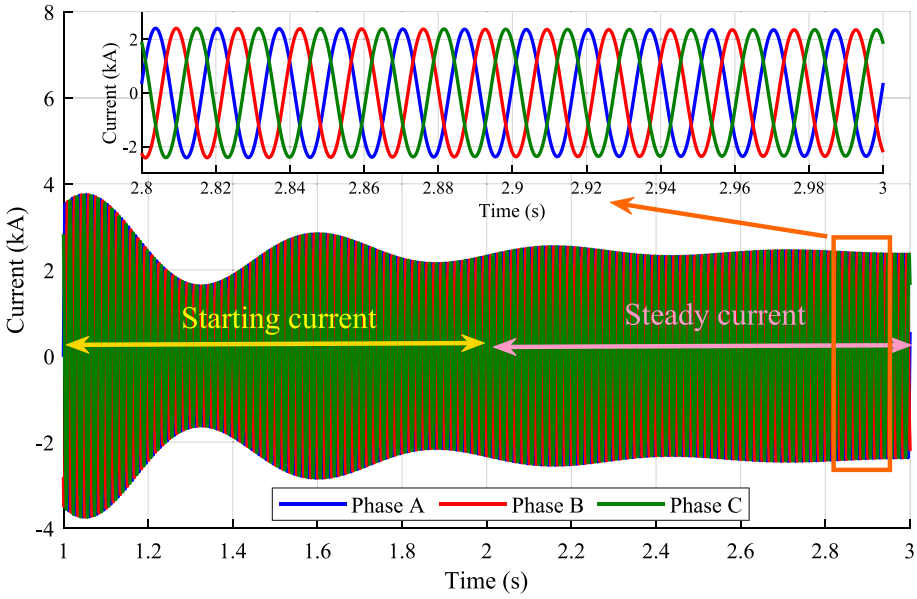

Fig. 5. The current of the power system under steady state and start-up current of the DGs.

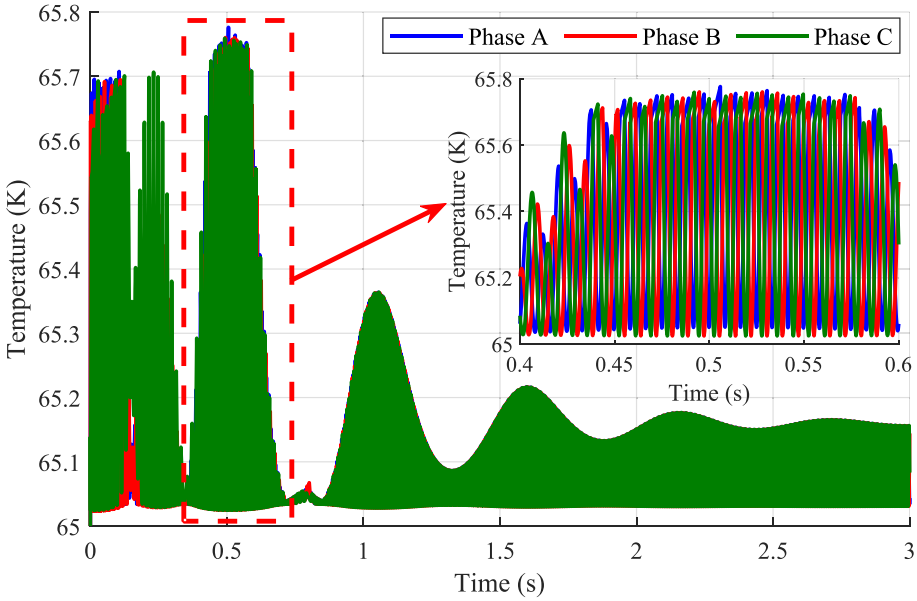

Fig. 6. Temperature characteristic of the HTS transformer with bare windings, under DG start-up current and steady state of the grid.

3.2. Fault tolerability concept for HTS transformer

In this section, the thermal characteristic of the HTS transformer affected by different fault currents at different locations of the power system is analysed. In this regard, three different scenarios are considered for the insulation method of the HTS windings on both the HV and LV sides. These scenarios include HTS windings with bare tapes, with Kapton insulated tapes, and with Acrylated Urethane solid insulation. Heat transfer regimes for HTS tapes with different insulations are shown in Fig. 8, based on the results presented in [44]. As shown in this figure, using insulated tapes in HTS windings increases the heat flux value during the nucleate boiling regime. The maximum heat flux value in the nucleate boiling regime for bare tape is 30 kW/m^2 while this value for Kapton insulated tape is about 80 kW/m^2 (166% increase). By using solid insulated tapes, this value is even further increased, and reaches 170 kW/m^2 which means a 112% increase compared to Kapton insulated tapes and a 460% increase compared to bare tapes. The data shown in Fig. 8 are experimentally measured and published in [44].

Fig. 9 displays the temperature profile of secondary windings of the HTS transformer, in phase A under the F1 fault scenario. When a fault happens, the temperature starts to rapidly increase, until the fault is cleared. After that, the temperature reduces until it gets back to the base temperature, i.e., 65 K. Due to the lower heat flux value of bare tapes, the windings temperature approaches to near 350 K which could increase the risk of HTS tape burnout. By using Kapton insulated tapes, the peak temperature of the HTS winding is 34% reduced while using solid insulated tapes could even further reduce the peak temper-

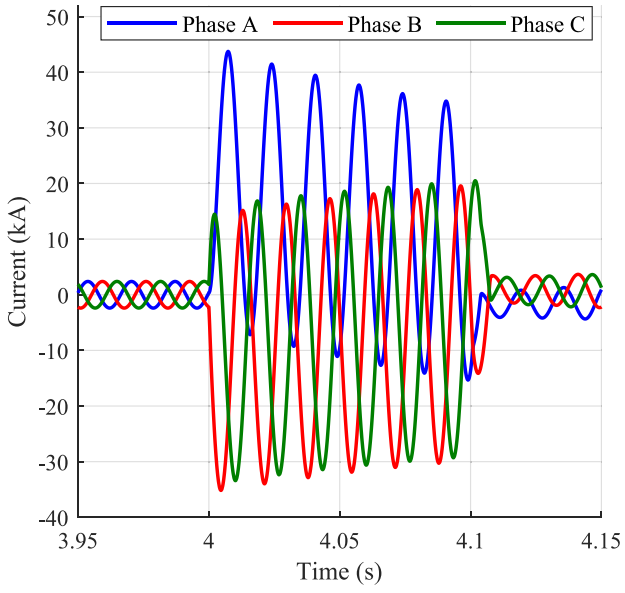

a) The fault current of each phase in fault scenario 1

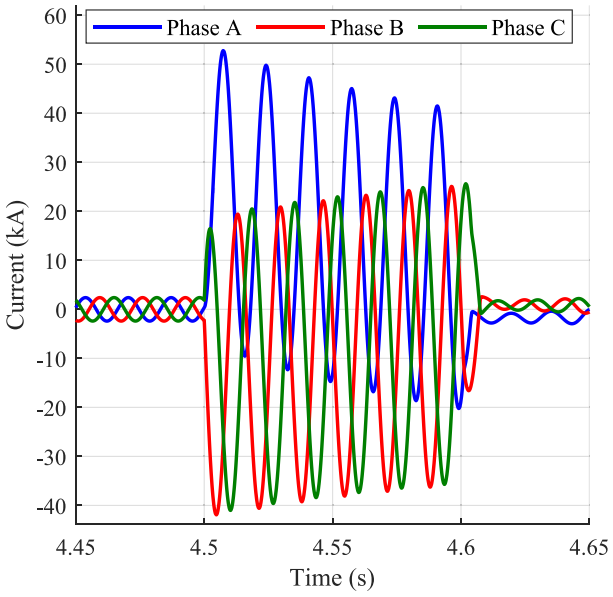

The fault current of each phase in fault scenario 2

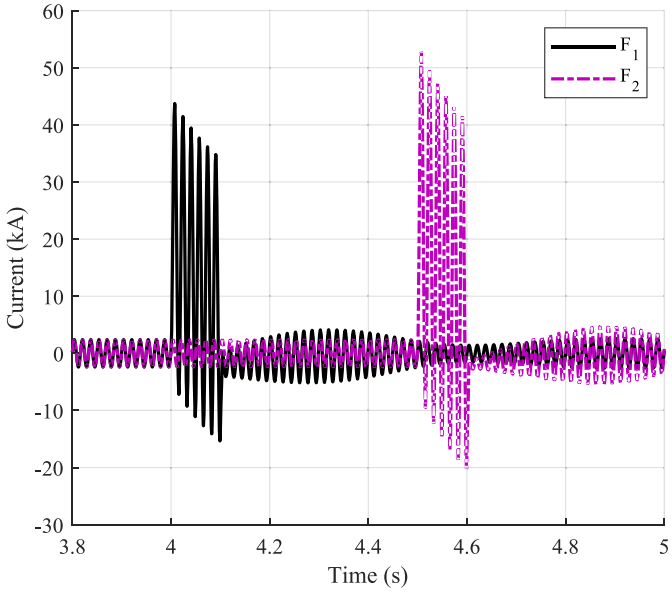

c) fault current profile in phase A for two fault scenarios

Fig. 7. Fault current characteristic for different fault scenarios in studied power system.

ature of HTS winding. Using Acrylated Urethane as insulation of HTS windings could 72% reduce the peak temperature. Since, insulations increase the heat flux value of the nucleate boiling regime, during a fault, more heat is transferred from the windings surface to cryogenic coolant fluid.

As shown in Fig. 10, F2 has more fault current than F1, the peak temperature of the secondary windings under this fault increases. Compared to F1 scenario, bare HTS windings experience a 35% temperature increase under the F2 fault scenario, which is 460 K, while this number for Kapton insulated windings and solid insulated windings is approximately equal to 28% and 20%, respectively. Bare tapes experience a 35% peak temperature increase while this value for Kapton insulated and solid insulated windings is about 27% and 21, respectively. However, even after the fault current increase imposed on HTS windings, the peak temperature of solid insulated HTS windings is about 150% and 310% lower than the peak temperature of Kapton insulated and bare windings, respectively. As a result of this, even under a higher fault current amplitude of F2, the HTS with solid insulated windings is still capable of providing the load for the MG2.

As shown in the above figures, solid insulated windings could tolerate fault current without any risk of burnouts and deformation. Based on this, the next step is investigating how loading after fault clearance could be tolerated by an HTS transformer.

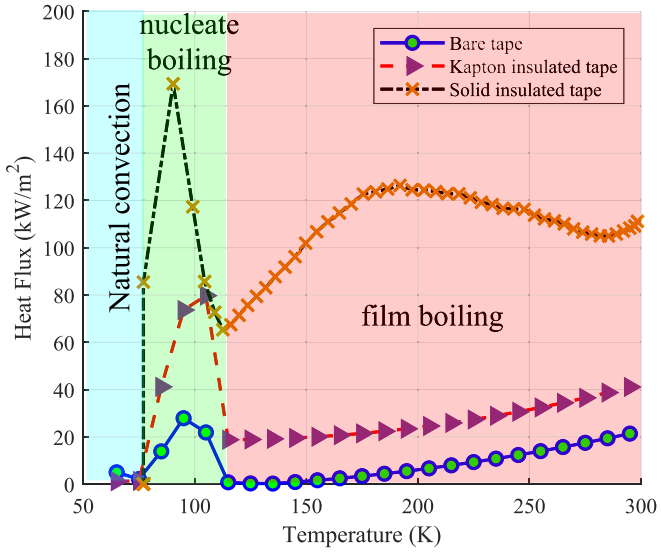

Fig. 8. Heat transfer regimes for HTS tape of transformer with different insulations.

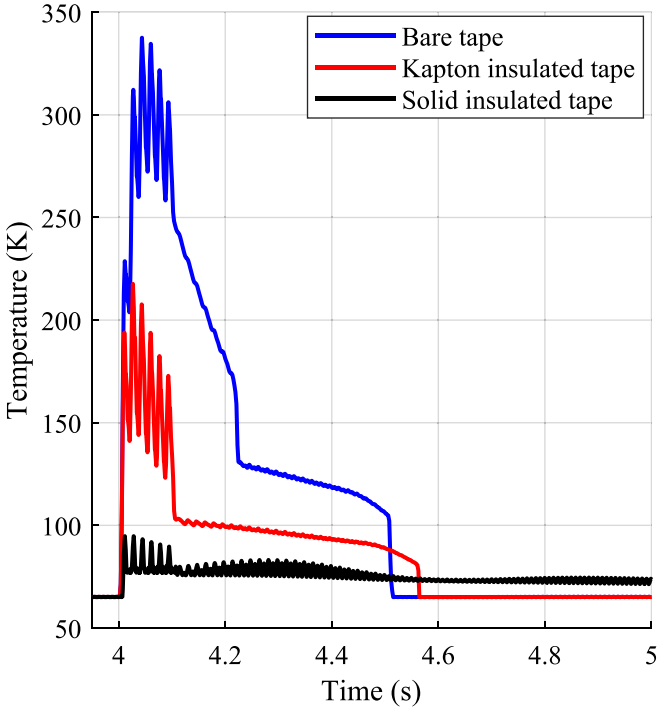

Fig. 9. Temperature characteristic of HTS transformer with different types of insulations, under F1 fault.

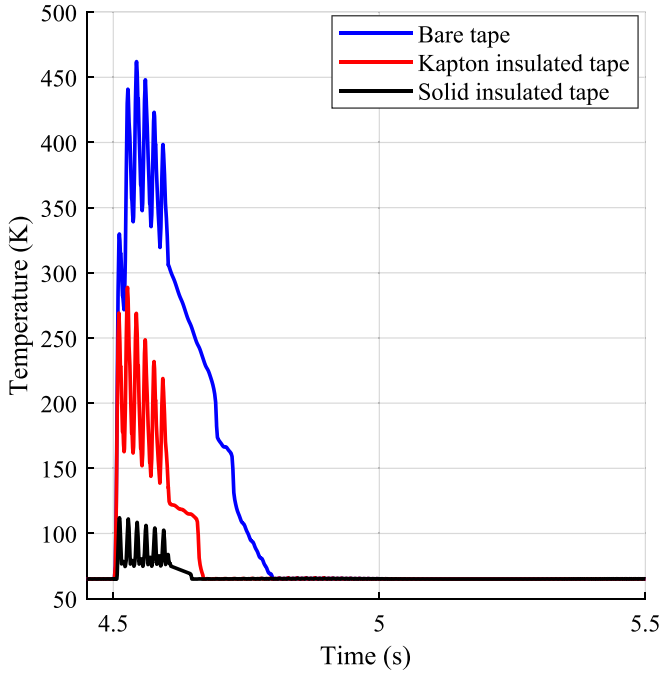

Fig. 10. Temperature characteristic of HTS transformer with different types of insulations, under F2 fault.

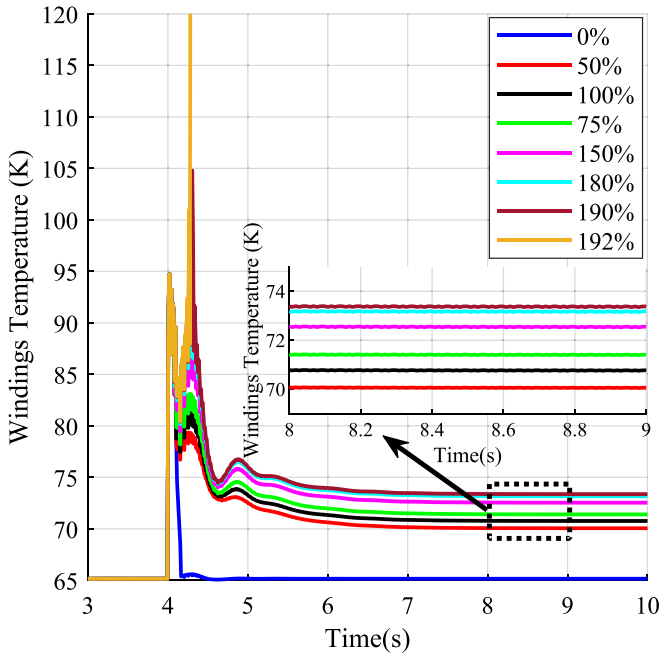

Fig. 11. Recovery under load characteristic of HTS transformer with solid insulation under F1 fault scenario.

3.3. Post-fault recovery of the HTS transformer

In this section, the impact of transformer loading after fault clearance is investigated to see how much energy could result in burnout or thermal runaway of HTS windings, after fault clearance. For this purpose, different loadings have been applied to the HTS transformer during its recovery state. These loadings are representative of healthy MG supply by HTS transformer, after fault clearance. In this regard, Fig. 11 shows the under-fault and post-fault performances of the HTS transformer caused by the F1 fault scenario. When there is no loading after fault clearance, HTS windings rapidly recover to base operational temperature. This state is known as full recovery where the temperature of HTS windings is equal to the base temperature of the cryogenic coolant, here, 65 K. There is also another stat known as partial recovery where the temperature of HTS windings is lower than critical temperature but still higher than base coolant temperature. As seen in Fig. 11, when loading after fault clearance is considered, HTS windings are not able to enter the full recovery zone, instead, they operate in a partial recovery state. Here the temperature quickly drops from peak temperature due to nucleate boiling but when reaches to natural conduction regime, it will drastically slow down

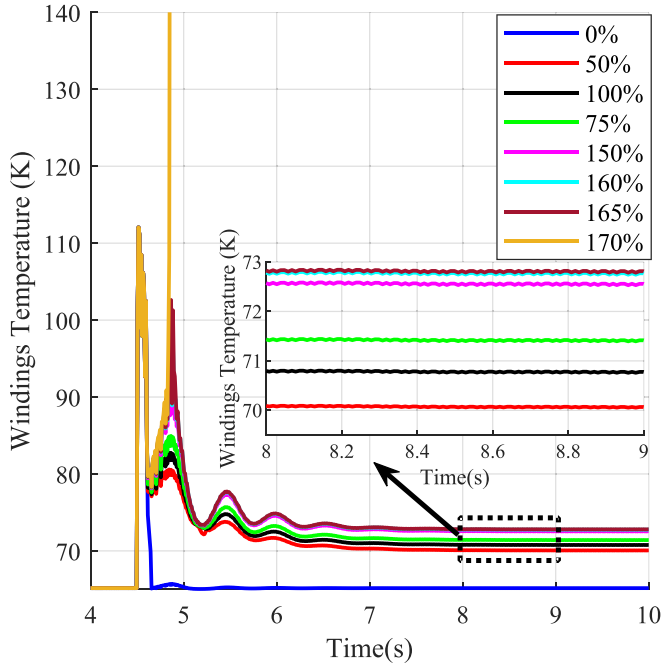

Fig. 12. Recovery under load characteristic of HTS transformer with solid insulation, fault 2.

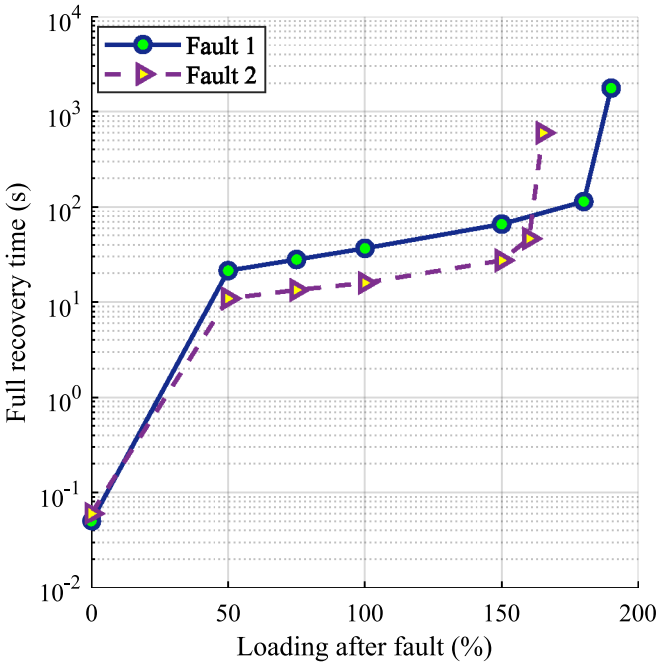

Fig. 13. Estimated full recovery time of HTS transformer winding using exponential fitting, under two fault scenarios.

[43]. By the increase of the post-fault loading, more electrical energy would be injected into HTS windings, and this results in increasing the full recovery time of windings. However, HTS windings have a maximum capacity where any further increase in the input energy results in the thermal runaway of HTS windings. In the case of the F1 fault scenario, this maximum capacity is 192% of rated loading which means that by imposing a current 1.92 times higher than the rated current, HTS windings would never recover, face thermal runaway, and their temperature would increase until their full burnout.

Fig. 12 shows the post-fault performance of the HTS transformer, under the F2 fault scenario where different loadings have been applied to the HTS transformer after fault is cleared. The previous trend could be seen in this figure with one difference where the maximum tolerable post-fault loading of the HTS transformer is approximately 11.5% reduced. This reduction originated in the higher fault current of the F2 scenario compared to the F1 scenario.

After investigating on the impact of the post-fault loading, a mathematical exponential fitting is used here to estimate the full recovery time of the HTS windings, under F1 and F2 fault scenarios. In this regard, the fitting parameters are shown in Table 5 and Table 6 of the paper, based on different scenarios of faults and their post-fault loading before thermal runaway.

Table 5
The Fitting parameters of recovery time for the F2 fault scenario.

Loading % after fault	Fit Equation $T(t) = a\exp(b \times t) + c\exp(d \times t)$			
	a	b	c	d
0	0	−18.5256	65.0709	0.0021
50	0.0003	−6.4355	70.5509	−0.0077
75	0.0013	−5.5195	71.1775	−0.0062
100	0.0032	−4.9786	71.7508	−0.0050
150	0.0108	−4.2908	72.7753	−0.0031
180	0.0192	−3.9795	73.3245	−0.0019
190	0.0362	−3.6547	73.4095	−0.0001

Table 6
The Fitting parameters of recovery time for the F2 fault scenario.

Loading % after fault	Fit Equation $T(t) = a\exp(b \times t) + c\exp(d \times t)$			
	a	b	c	d
0	0.0001	−18.5783	65.0228	0.0033
50	0.0002	−13.5252	71.0423	−0.0171
75	0.0004	−10.8429	71.6874	−0.0155
100	0.0004	−8.1846	72.1846	−0.0125
150	0.0024	−5.4080	73.0522	−0.0074
160	0.0072	−4.7501	73.1528	−0.0055
165	0.0119	−4.4606	73.1323	−0.0045

Fig. 13 shows the estimated full recovery time of HTS windings under different fault scenarios concerning the variations of the loading. As can be seen, when loading increases from 0% to 50%, an abrupt change is observable while after that increasing the post-fault loading, increases the recovery time of the HTS windings. Finally, before the thermal runaway of the HTS windings, the full recovery time is

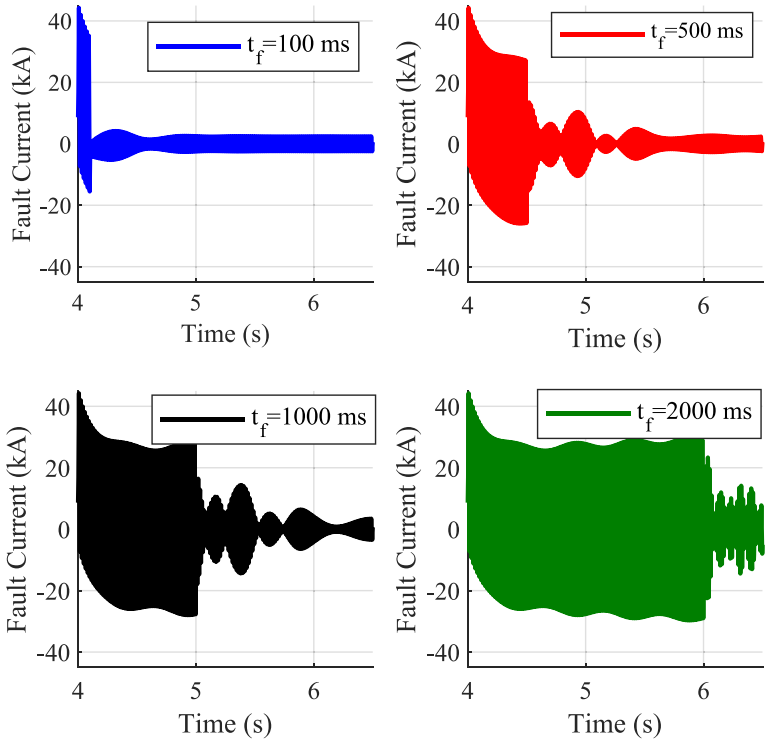

a)

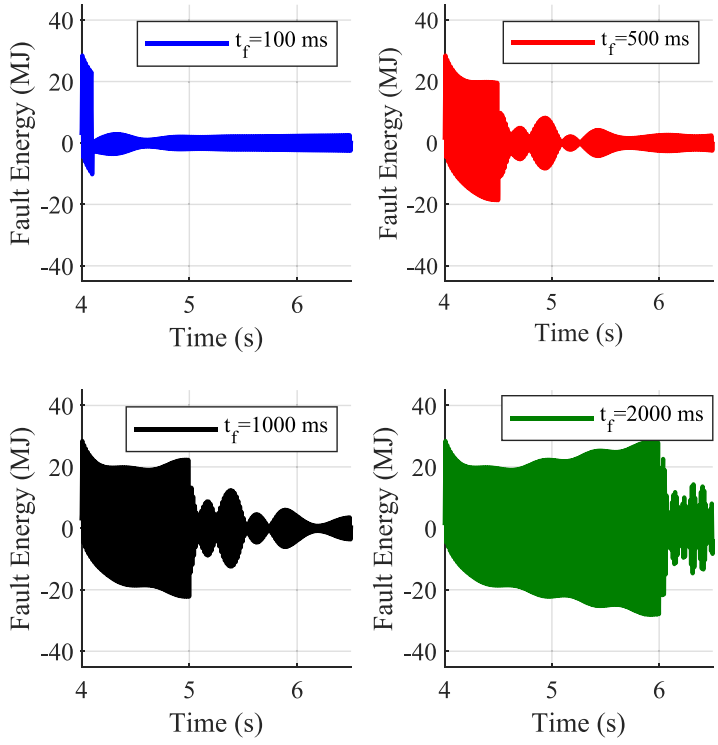

b)

Fig. 14. Faults with different durations, a) fault current, b) fault energy.

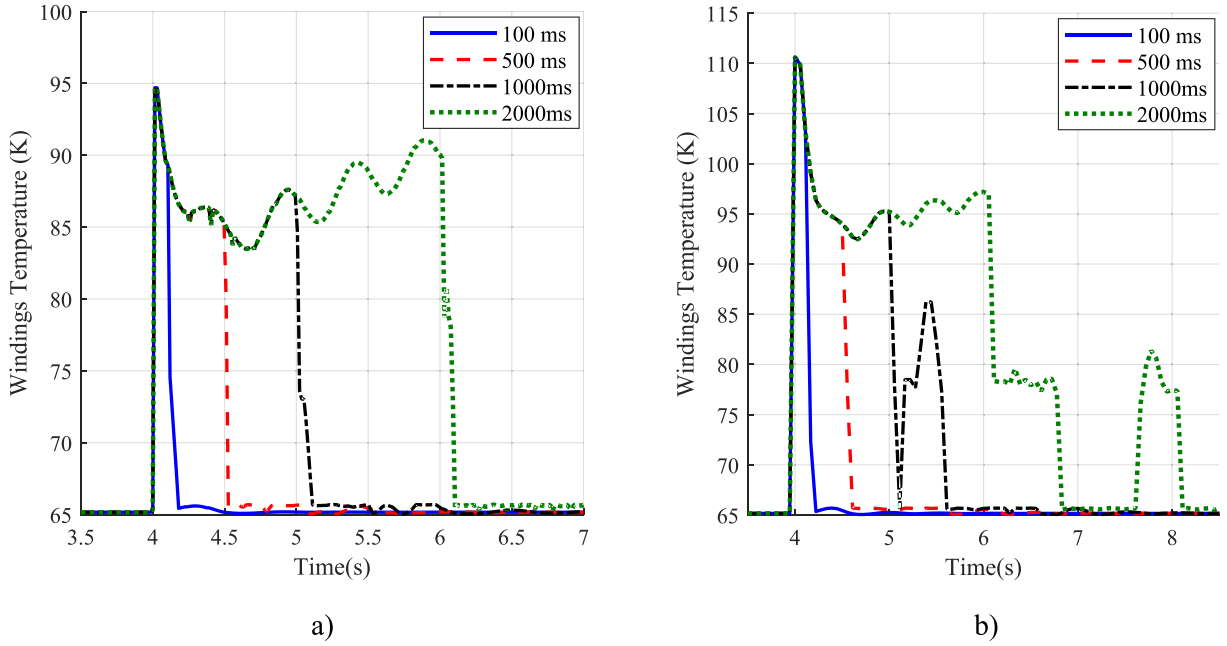

Fig. 15. Temperature characteristic of the solid insulated HTS transformer, under different lengths of fault.

increased abruptly again to around half an hour. This again shows why any further increase in post-fault loading results in the thermal runaway of the HTS windings.

The next step in the system analysis of the FTCL HTS transformer is to investigate the impact of long-duration faults on the thermal characteristics of the HTS windings. For this purpose, four fault durations have been considered for each fault scenario which include, 100 ms, 500 ms, 1000 ms, and 2000 ms, as shown in Fig. 14(a). The amount of fault energy imposed on the HTS windings during and after the fault is shown in Fig. 14(b).

Fig. 15 shows the temperature profile of the secondary windings of phase A, under different fault durations. As seen in this figure, by increasing the duration of the fault current, the peak temperature does not change. Because, after the first peak of the fault current, the amount of energy injected into the HTS windings is reduced so the temperature of HTS windings reduces. In case of 2 second fault, the fault energy is accumulated again and causes the temperature increase of the HTS windings, after reduction.

It should be mentioned that our proposed model for HTS transformer, as indicated in reference [45], demonstrates effective coping with experimental results. However, challenges exist, particularly in the context of system-level analysis for electric grids. While the proposed model exhibits speed advantages when compared to Finite Element Method (FEM)-based approaches, its computational time is depending on the chosen time step. For system-level analysis, scenarios may exist where transients with time steps less than a microsecond. Addressing such transients becomes imperative, as the computational time even for fast methods, like the proposed one, experiences a significant increase. A challenge lies in the fact that transformer models establish by primarily focusing on heat transfer experimental data extracted from component level testing, that is because of absence of experimental heat transfer results for MW-level winding heat transfer. To surmount these challenges, Artificial Intelligence (AI)-based surrogate models [30,57,58] come into play. These surrogate models establish a logical relationship between inputs (system variables) and outputs (system characteristics), bypassing the need to solve complex electromagnetic and thermomechanical equations. Generally characterized by their speed, these models offer faster computational times, with their accuracy tied to the precision of the underlying model.

4. Conclusion

High Temperature Superconducting (HTS) transformers will play a promising role in future power grids where most of the electrical power is generated by clean energy sources, such as wind farms and solar farms. HTS transformers offer 50% lower weight and size, lower energy losses, massive overloading capacity, and fault-tolerant characteristics. Indeed, Fault Tolerant Current Limiting HTS (FTCL HTS) transformers are novel types of HTS transformers that could endure fault currents. However, the system-level study of FTCL HTS transformers was never investigated. In this paper, a 132/13.8 kV, 50 MVA FTCL HTS transformer was implemented into a standard IEEE power system in the presence of distributed generation units. Then, the fault performance of the FTCL HTS transformer is studied, where the most important findings of this paper are:

- By using the bare tapes in HTS windings, the peak temperature of these windings increases, in the range of 340 K to 450 K, under different fault scenarios.
- Covering the HTS tapes with Kapton insulation papers, causes the peak temperature reduction of HTS windings in the range of 220 K to 270 K, under different fault scenarios.
- Substantial reduction in peak temperature of HTS windings is achieved when Acrylated Urethane insulations are used where the peak temperature ranges between 95 K to 110 K, for different fault scenarios.
- The Acrylated Urethane-insulated HTS transformer could also endure 170% to 192% post-fault overloading, without any risk of HTS tape burnout.
- Imposing the loading and overloading, after fault clearance, increases the full recovery time of HTS windings while the partial recovery time is still low.

Declaration of competing interest

The authors declare that they have no known competing financial interests or personal relationships that could have appeared to influence the work reported in this paper.

Acknowledgements

For open access, the author(s) has applied a Creative Commons Attribution (CC BY) license to any Author Accepted Manuscript version arising from this submission.

References

[1] Fankhauser S et al. The meaning of net zero and how to get it right. Nat Clim Chang 2022;12(1):15–21. https://doi.org/10.1038/s41558-021-01245-w.
[2] Bistline JET, Blanford GJ. The role of the power sector in net-zero energy systems. Energy Climate Change 2021;2:100045. https://doi.org/10.1016/j.egycc.2021.100045.
[3] Moghaddasi H, Culp C, Vanegas J. Net zero energy communities: integrated power system, building and transport sectors. Energies (Basel) 2021;14(21):7065. https://doi.org/10.3390/en14217065.
[4] Giampieri A, Ling-Chin J, Roskilly AP. Techno-economic assessment of offshore wind-to-hydrogen scenarios: a UK case study. Int J Hydrogen Energy 2023. https://doi.org/10.1016/j.ijhydene.2023.01.346.
[5] Glasson N et al. Test results and conclusions from a 1 MVA superconducting transformer featuring 2G HTS roebel cable. IEEE Trans Appl Supercond 2017;27(4):1–5. https://doi.org/10.1109/TASC.2016.2639032.
[6] Sadati SMB, Darvish Motevali B, Dargahi M, Yazdani-Asrami M. Evaluation of distribution transformer Losses and remaining life considering network harmonic, based on analytical and simulation methods. Austr J Basic Appl Sci (AJBAS) 2010;4(10):5291–9.
[7] Yazdani-Asrami M, Mirzaie M, Shayegani Akmal AA. No-load loss calculation of distribution transformers supplied by nonsinusoidal voltage using three-dimensional finite element analysis. Energy 2013;50:205–19. https://doi.org/10.1016/j.energy.2012.09.050.
[8] Berger A, Cherevatskiy S, Noe M, Leibfried T. Comparison of the efficiency of superconducting and conventional transformers. J Phys Conf Ser 2010;234(3):032004. https://doi.org/10.1088/1742-6596/234/3/032004.
[9] Mike S, Enric P, Liam J, Mohinder P, Neil G. Prospects for HTS transformers in the grid: AC loss and economics. In *EUCAS*; 2015.
[10] Mike S, et al. Cooling systems for HTS transformers: impact of cost, overload, and fault current performance expectations. In: *2nd International Workshop on Cooling Systems for HTS Applications (IWC-HTS)*, Karlsruhe; 2017.
[11] Yazdani-Asrami M et al. Insulation materials and systems for superconducting powertrain devices in future Cryo-electrified aircraft: part I—material challenges and specifications, and device-level application. IEEE Electr Insul Mag 2022;38(2):23–36. https://doi.org/10.1109/MEI.2022.9716211.
[12] Pronto AG, Neves MV, Rodrigues AL. Measurement and separation of magnetic losses at room and cryogenic temperature for three types of steels used in HTS transformers. J Supercond Nov Magn 2011;24(1–2):981–5. https://doi.org/10.1007/s10948-010-0867-9.
[13] Yazdani-Asrami M et al. Influence of field-dependent critical current on harmonic AC loss analysis in HTS coils for superconducting transformers supplying non-linear loads. Cryogenics (Guildf) 2021;113:103234. https://doi.org/10.1016/j.cryogenics.2020.103234.
[14] Ghabeli A et al. Optimization of distributive ratios of apportioned winding configuration in HTS power transformers for hysteresis loss and leakage flux reduction. J Supercond Nov Magn 2015;28(12):3463–79. https://doi.org/10.1007/s10948-015-3165-8.
[15] Song W et al. AC loss simulation in a HTS 3-Phase 1 MVA transformer using H formulation. Cryogenics (Guildf) 2018;94:14–21. https://doi.org/10.1016/j.cryogenics.2018.07.003.
[16] Song W et al. Design of a single-phase 6.5 MVA/25 kV superconducting traction transformer for the Chinese Fuxing high-speed train. Int J Electr Power Energy Syst 2020;119:105956. https://doi.org/10.1016/j.ijepes.2020.105956.
[17] Song W et al. AC loss effect of high-order harmonic currents in a single-phase 6.5 MVA HTS traction transformer. IEEE Trans Appl Supercond 2019;29(5):1–5. https://doi.org/10.1109/TASC.2019.2901014.
[18] Jiang Z et al. 15% reduction in AC loss of a 3-phase 1 MVA HTS transformer by exploiting asymmetric conductor critical current. J Phys Commun 2021;5(2):025003. https://doi.org/10.1088/2399-6528/abe036.
[19] Song W et al. AC loss calculation on a 6.5 MVA/25 kV HTS traction transformer with hybrid winding structure. IEEE Trans Appl Supercond 2020;30(4):1–5. https://doi.org/10.1109/TASC.2020.2975771.
[20] Song W et al. Role of flux diverters in reducing AC loss in a single-phase 6.5 MVA HTS traction transformer for Chinese high-speed train carrying high-order harmonic currents. IEEE Access 2022;10:69650–8. https://doi.org/10.1109/ACCESS.2022.3186858.
[21] Fang X et al. Application of flux diverters in high temperature superconducting transformer windings for AC loss reduction. IEEE Trans Appl Supercond 2021;31(8):1–5. https://doi.org/10.1109/TASC.2021.3108734.
[22] Wu Y et al. Combined impact of asymmetric critical current and flux diverters on AC loss of a 6.5 MVA/25 kV HTS traction transformer. IEEE Trans Transp Electrif 2023;9(1):1590–604. https://doi.org/10.1109/TTE.2022.3194027.
[23] Liao X et al. Analysis of electromagnetic characteristics of 6.5 MVA/25 kV HTS traction transformer using *T-A* formulation. IEEE Trans Appl Supercond 2023;33(4):1–8. https://doi.org/10.1109/TASC.2022.3190365.
[24] Zhao X et al. Design, development, and testing of a 6.6 MVA HTS traction transformer for high-speed train applications. Supercond Sci Technol 2023;36(8):085009. https://doi.org/10.1088/1361-6668/acdcbf.
[25] Pardo E et al. AC loss modelling and measurement of superconducting transformers with coated-conductor Roebel-cable in low-voltage winding. Supercond Sci Technol 2015;28(11):114008. https://doi.org/10.1088/0953-2048/28/11/114008.
[26] Glasson ND et al. Verification testing for a 1 MVA 3-phase demonstration transformer using 2G-HTS roebel cable. IEEE Trans Appl Superconduct 2013;23(3):5500206. https://doi.org/10.1109/TASC.2012.2234919.
[27] Glasson N et al. Risk mitigation in the development of a roebel cable based 1 MVA HTS transformer. Phys Proc 2012;36:830–4. https://doi.org/10.1016/j.phpro.2012.06.135.
[28] Pronto AG, Maurício A, Pina JM. Magnetic properties measurement and discussion of an amorphous power transformer core at room and liquid nitrogen temperature. J Phys Conf Ser May 2014;507(3):032018. https://doi.org/10.1088/1742-6596/507/3/032018.
[29] Mahamed M et al. Impact of Perlator on the cooling liquid flow and hottest point temperature of superconducting windings in HTS transformer. Superconductivity 2022;3:100021. https://doi.org/10.1016/j.supcon.2022.100021.
[30] Yazdani-Asrami M et al. Roadmap on artificial intelligence and big data techniques for superconductivity. Supercond Sci Technol 2023;36(4):043501. https://doi.org/10.1088/1361-6668/acbb34.
[31] Yazdani-Asrami M et al. Artificial intelligence for superconducting transformers. Transformer Magazine 2021;8(S5):22–30.
[32] Janowski T et al. Fault current limitation in power network by the superconducting transformers made of 2G HTS. IEEE Trans Appl Supercond 2011;21(3):1413–6. https://doi.org/10.1109/TASC.2011.2112325.
[33] Abdul Rahman MA, Lie TT, Prasad K. Performance analysis of HTS transformer with fault current limiting properties on short circuit current. In: 2011 International Conference on Applied Superconductivity and Electromagnetic Devices. IEEE; 2011. p. 54–7. , https://doi.org/10.1109/ASEMD.2011.6145066.
[34] Jaroszynski L, Wojtasiewicz G, Janowski T. Considerations of 2G HTS transformer temperature during short circuit. IEEE Trans Appl Supercond 2018;28(4):1–5. https://doi.org/10.1109/TASC.2018.2806561.
[35] Abdul Rahman MA, Lie TT, Prasad K. The effects of short-circuit and inrush currents on HTS transformer windings. IEEE Trans Appl Superconduct 2012;22(2):5500108. https://doi.org/10.1109/TASC.2011.2173571.
[36] Janowski T, Wojtasiewicz G. Possibility of using the 2G HTS superconducting transformer to limit short-circuit currents in power network. IEEE Trans Appl Superconduct 2012;22(3):5500804. https://doi.org/10.1109/TASC.2011.2174570.
[37] Pi W et al. Fault current characteristics of parallel stainless steel & REBCO tapes and a 6 kV/400 V HTS transformer. IEEE Trans Appl Supercond 2021;31(5):1–6. https://doi.org/10.1109/TASC.2021.3066248.
[38] Elshiekh M et al. Effectiveness of superconducting fault current limiting transformers in power systems. IEEE Trans Appl Supercond 2018;28(3):1–7. https://doi.org/10.1109/TASC.2018.2805693.
[39] Hayakawa N et al. Progress in development of superconducting fault current limiting transformer (SFCLT). IEEE Trans Appl Supercond 2011;21(3):1397–400. https://doi.org/10.1109/TASC.2010.2089412.
[40] Omura K et al. Current limiting characteristics of parallel-connected coated conductors for high-Tc superconducting fault current limiting transformer (HTc-SFCLT). IEEE Trans Appl Supercond 2009;19(3):1880–3. https://doi.org/10.1109/TASC.2009.2018067.
[41] Hellmann S et al. Manufacturing of a 1-MVA-class superconducting fault current limiting transformer with recovery-under-load capabilities. IEEE Trans Appl Supercond 2017;27(4):1–5. https://doi.org/10.1109/TASC.2017.2652493.
[42] Hellmann S et al. Current limitation experiments on a 1 MVA-class superconducting current limiting transformer. IEEE Trans Appl Supercond 2019:1. https://doi.org/10.1109/TASC.2019.2906804.
[43] Yazdani-Asrami M et al. Fault current limiting HTS transformer with extended fault withstand time. Supercond Sci Technol 2019;32(3):035006. https://doi.org/10.1088/1361-6668/aaf7a8.
[44] Yazdani-Asrami M, Staines M, Sidorov G, Eicher A. Heat transfer and recovery performance enhancement of metal and superconducting tapes under high current pulses for improving fault current-limiting behavior of HTS transformers. Supercond Sci Technol 2020;33(9):095014. https://doi.org/10.1088/1361-6668/aba542.
[45] Yazdani-Asrami M et al. Role of insulation materials and cryogenic coolants on fault performance of MW-scale fault-tolerant current-limiting superconducting transformers. IEEE Trans Appl Supercond 2023;33(1):1–15. https://doi.org/10.1109/TASC.2022.3217967.
[46] Katiraei F, Iravani MR, Lehn PW. Micro-grid autonomous operation during and subsequent to islanding process. IEEE Trans Power Delivery 2005;20(1):248–57. https://doi.org/10.1109/TPWRD.2004.835051.
[47] Menon V, Nehrir MH. A hybrid islanding detection technique using voltage unbalance and frequency set point. IEEE Trans Power Syst 2007;22(1):442–8. https://doi.org/10.1109/TPWRS.2006.887892.
[48] Duron J et al. Modelling the E-J relation of high-Tc superconductors in an arbitrary current range. Phys C Supercond 2004;401(1–4):231–5. https://doi.org/10.1016/j.physc.2003.09.044.
[49] Zhao X et al. Design, development, and testing of a 6.6 MVA HTS traction transformer for high-speed train applications. Supercond Sci Technol 2023;36(8):085009. https://doi.org/10.1088/1361-6668/acdcbf.

[50] Lapthorn A, Bodger P, Enright W. A 15-kVA high-temperature superconducting partial-core transformer—Part 1: transformer modeling. IEEE Trans Power Delivery 2013;28(1):245–52. https://doi.org/10.1109/TPWRD.2012.2226478.
[51] Wang J et al. Derivation, calculation and measurement of parameters for a multi-winding transformer electrical model. In: APEC '99. Fourteenth Annual Applied Power Electronics Conference and Exposition. 1999 Conference Proceedings (Cat. No.99CH36285). IEEE; 1999. p. 220–6. , https://doi.org/10.1109/APEC.1999.749513.
[52] Volkov EP et al. First 1 MVA and 10/0.4 kV HTSC transformer in Russia. Therm Eng 2016;63(13):909–16. https://doi.org/10.1134/S0040601516130085.
[53] Morandi A et al. Superconducting transformers: key design aspects for power applications. J Phys Conf Ser 2008;97:012318. https://doi.org/10.1088/1742-6596/97/1/012318.
[54] Xiang B et al. Study on the influencing factors to reduce the recovery time of superconducting tapes and coils for the DC superconducting fault current limiter applications. High Voltage 2022;7(3):483–95. https://doi.org/10.1049/hve2.12158.
[55] Sadeghi A, Seyyedbarzegar S, Yazdani-Asrami M. Investigation on the electrothermal performance of a high-temperature superconducting cable in an offshore wind farm integrated power system: fault and islanding conditions. IEEE Trans Appl Supercond 2022;32(8):1–11. https://doi.org/10.1109/TASC.2022.3196770.
[56] Kalsi SS. Applications of high temperature superconductors to electric power equipment. Wiley; 2011. , https://doi.org/10.1002/9780470877890.
[57] Yazdani-Asrami M. Artificial intelligence, machine learning, deep learning, and big data techniques for the advancements of superconducting technology: a road to smarter and intelligent superconductivity. Supercond Sci Technol 2023;36(8):084001. https://doi.org/10.1088/1361-6668/ace385.
[58] Yazdani-Asrami M et al. Artificial intelligence methods for applied superconductivity: material, design, manufacturing, testing, operation, and condition monitoring. Supercond Sci Technol 2022;35(12):123001. https://doi.org/10.1088/1361-6668/ac80d8.